*Korean J. Chem. Eng.*, **25**(5), 1170-1177 (2008)

# Hydrodynamic characteristics of activated carbon in air- and water-fluidized beds

**Aurél Ujhidy†, György Bucsky, and Jenö Németh**

Research Institute of Chemical and Process Engineering, University of Pannonia, Veszprém 8200, Hungary
(*Received 12 July 2007 • accepted 7 February 2008*)

**Abstract**−The hydrodynamic characteristics of small hydrophobic activated carbon particles were determined in air flowing through both fixed and fluidized bed layers and water flowing through an inverse fluidized bed. Based on experimental data the Ergun-equation was corrected. A new relationship is proposed to predict the pressure drop in a fixed bed with gas flowing by using the minimum fluidizing velocity ($u_{mf}$) and particle terminal velocity ($u_t$). Apparent density of oven-dried activated carbon increases with filling the internal pores by water. After the bed density reaches the density of water, the system switches from an inverse fluidized layer into the classical fluidized state. Finally, it has been demonstrated that the Reynolds number ($Re_{mf}$) at $u_{mf}$ associated with the original Archimedes number (Ar) for gas-solid fluidized system and the modified Ar numbers characterizing the inverse fluidized beds lie on identical curves.

Key words: Inverse Fluidized Bed, Activated Carbon, Hydrodynamic Characteristics

## INTRODUCTION

Normally, solid particles can be fluidized by the upward flow of gas or liquid, but the nature of bed expansion will differ with the two different fluidizing media [1]. Anderson et al. [2] have proven theoretically that, in contrast to a gas/solid fluidized bed, bubbles cannot form in a liquid/solid fluidized bed.

The apparent density ($\rho_a$) of particles with internal pores (catalysts, adsorbents) is often lower than that of liquid. In such cases, the fluidizing condition may become an inverse fluidized bed (IFB). During inverse fluidization, particles are suspended against buoyancy and drag force in the liquid flowing downwards as a continuous phase. If three phases are present instead of two phases, then bubbling gas flows upwards in a counter-flow with the liquid forming a continuous phase that is known as an inverse three-phase fluidized bed. The advantages of IFB are low pressure drop, higher heat and mass transfer rates between the phases, low solids attrition, simple control of the biofilm thickness, and easy restart of the system. Major areas of application of two and three-phase IFB are catalytic reactions, mainly in petrochemistry and biotechnology, as well as the biological treatment of waste water [3-6].

The hydrodynamics of two-phase IFB reactors have been reported in the literature in the various operating flow regimes [7-13], but clear-cut design principles are still lacking. For example, several publications have dealt with bed expansion [8,9], but the proposed correlations to predict bed expansion are only valid within limited ranges. Hydrodynamic conditions of three-phase fluidized bed systems have been elaborated more thoroughly than for two-phase IFB systems, but there are still no acceptable methods available even in this area.

As far as design of the bed is concerned, Comte et al. [14] and Epstein et al. [15] have proposed usable methods to determine the effect of distributors to delimit the fluidized bed on gas holdup and on the possibilities for eliminating mal-distributions of the flowing media. Renganathan et al. [12] proposed the classification of fluidized beds by measuring the local voidage factor.

To the best of our knowledge, no data has been published so far on the inverse fluidized bed of activated carbon. Information is available on fluidized adsorbents for the adsorptive separation of gases and solvent vapors [1,16], but in these methods, gas or air flows through the activated carbon bed.

Impregnation of the activated carbon, with potassium iodide, acids or metallic oxides, for example, has a favorable effect on the selectivity characteristics of the adsorbent, or on its property of improving catalytic oxidation. The mass increase which occurs during the impregnation of activated carbon by water, in a similar way to an increase in biomass, has an effect on the hydrodynamic characteristics of the fluidized bed. The majority of these effects, however, have not yet been clarified.

The increase in the apparent density of particles, such as FCC catalysts with internal pores, is an undesirable phenomenon during the fluidized bed operation. Lewis and Bowerman [17], for instance, eliminated the problem of mass increase by first impregnating the catalyst particles with n-heptane. Certain surface properties of the plastic granules often used in the inverse fluidization experiments, such as the plasticizing component may also be disturbing ones. Comte et al. [14] eliminated this problem by the prior water treatment of the particles. While investigating the hydrophobic or hydrophilic nature of various PE granules, Han et al. [4] changed the hydrophobic character to hydrophilic by using a special chemical treatment. Due to the complicated hydrodynamic conditions of IFB, however, they deem further research in this area is needed.

Unlike silica gels or molecular sieves, activated carbon as an adsorbent is intrinsically hydrophobic. This is most likely the reason why activated carbon has not been chosen as a model material for IFB systems. The object of the present study is to find how the hydrophobic activated carbon can be fluidized by water compared to the equations obtained from the experiments with air and to establish the hydrodynamic equations which can be used to quantify the wet impregnation of activated carbon in a fluidized bed.

## EXPERIMENTAL

†To whom correspondence should be addressed.
E-mail: ujhidy@mukki.richem.hu

## 1. Apparatus

Two types of apparatus were used for the hydrodynamic experiments. A fixed and a fluidized bed of activated carbon particles were fluidized by air carried out in a glass tube with an internal diameter of D=0.052 m. Uniform air distribution was ensured by placing a sintered glass filter (Schott Duran® P250) at the bottom of the column. The bed pressure along the bed height was measured at pressure taps of 50 mm height intervals from the distributor. The particle size (0.90-2.2 mm) and the initial bed height (40-280 mm) were varied. The voidage factor of the fixed bed was close to a constant value from the repeated measurements. The bulk density of the fixed bad (e.g., 480±5 kg/m$^3$) was nearly constant, too (see Table 1). Further details of the apparatus can be found elsewhere [18].

The experimental setup is schematically shown in Fig. 1 for the liquid/activated carbon system. The liquid circulates through column (1) having an internal diameter of D=0.13 m. The particle stack in the column consists of 5 kg of Silicarbon 0.8 Supra activated carbon in a space delimited by two grids. Data collection is initiated by starting a circulation pump (2). The impregnation liquid (tap water) flows through a filter (3) and a cooler (4), and is homogenized in a mixing tank (5) if required, or recycled in the volume measured by a rotating flow meter (6). The liquid is fed cyclically either at the top or at the bottom of the column. Four microwave devices (7) were also installed along the height of the column with power output of 700 W each.

**Table 1. Properties of the solids**

| Type | đ | Density, kg/m$^3$ | | | Pore volume |
|---|---|---|---|---|---|
| | mm | $\rho_T$ | $\rho_a$ | $\rho_B$ | cm$^3$/g |
| BAU | 2 | 1950 | 436 | 192 | 0.854 |
| Nuxit BO | 0.715 | 2240 | 685 | 369 | 0.912 |
| | 0.90 | 2240 | 682 | 371 | 0.912 |
| Chemviron BPL | 2.2 | 2100 | 780 | 480 | 0.820 |
| Silicarbon 0.8 Supra | 1.15 | 2150 | - | 450 | 0.620 |

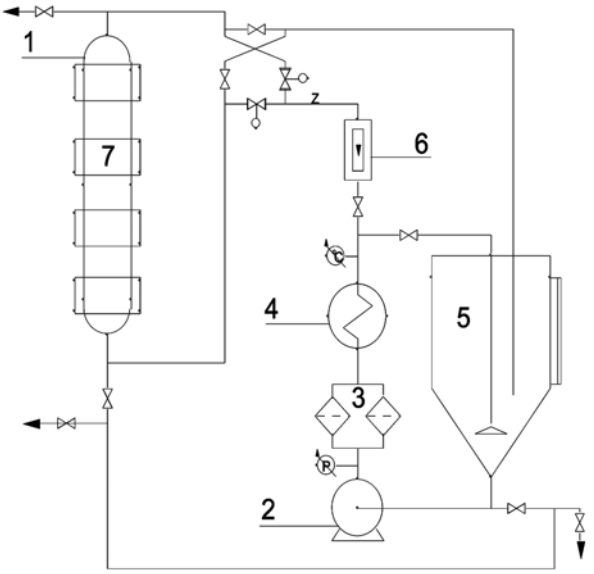


**Fig. 1. Schematic diagram of the apparatus.**

1. Column
2. pump
3. Filter
4. Cooler
5. Mixing tank
6. Flow meter
7. Microwave device

## 2. Experimental Procedure and Materials

Initially, the fluidizing liquid enters the column from the top and inversely fluidizes the activated carbon that is lighter than water. To impregnate the vesicles of the activated carbon more efficiently, the direction of water flow was altered after 5 min, and water was fed through the bed from the bottom for a further 5 min. At the same time, the computer-controlled microwave devices were switched on, one after the other, for 5 s at a time from bottom to top. When the uppermost microwave device switches off, the lowermost one is switched on again. The electromagnetic field intensifies the exchange of air and the flowing liquid in the internal vesicle of the activated carbon. This effect is based on the different relative permeability of water and air as a function of absorbed microwave energy at different extents. Activated carbon itself behaves differently in an electromagnetic field. The pressure exerted by the microwave radiation, and consequently the exchange of material, is also increased by the gas pressure fluctuation generated by the microwave heat, thus offsetting the hydrophobic nature of activated carbon.

After 5 min of the intensive treatment of microwave radiation, the flow was directed downwards and the bed was inversely fluidized. Observations indicate that approximately 50 min was required for a sufficient impregnation of the carbon vesicles. Following this, the particle bed, having become heavier than water, displays the homogeneous fluidization characteristics of the classical liquid/solid systems.

Four types of activated carbon were employed, namely the Russian BAU, the Hungarian Nuxit BO and the American Chemviron BPL which were finely ground with narrow size fractions, while the German Silicarbon 0.8 Supra activated carbon grains can be regarded as spheres. For the first three carbon types, the fluidization characteristics of the gas/solid system were tested, while for the fourth one, the hydrodynamic properties of liquid impregnation were determined. The main characteristics of the types are shown in Tables 1-3.

The equilibrium impregnation of activated carbon is given by the isothermal curves as a function of the partial pressures of the adsorbate. In the Brunauer-Emmet-Teller (BET) designation system, the water vapor isotherm on activated carbon is typically a type V isotherm (Fig. 2). As can be seen from the figure, the micropores

**Table 2. Pressure drop on a 1 m high fixed bed at a gas flow rate of 0.2 m/s**

| Type | Pressure drop, mbar |
|---|---|
| BAU | 19 |
| Nuxit BO (Ø,9 mm) | 3,1 |
| Chemviron BPL | 28 |
| Silicarbon | 10 |

**Table 3. Shape factors of Nuxit BO activated carbon**

| đ, mm | 0.408 | 0.715 | 0.90 | 1.8 |
|---|---|---|---|---|
| $\Psi$[-] | 0.7 | 0.61 | 0.59 | 0.54 |

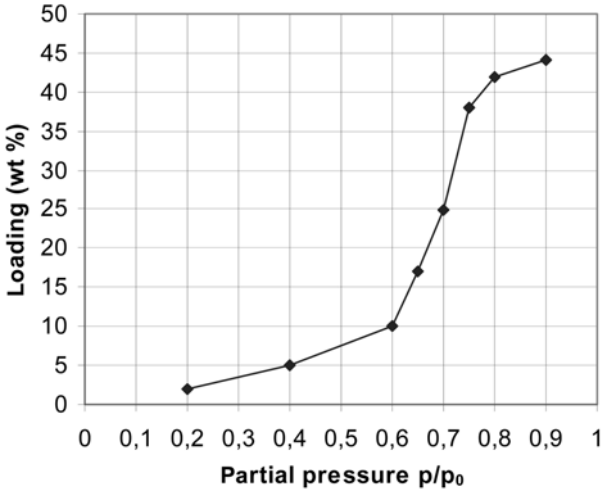


**Fig. 2. Adsorption of water from air by Silicarbon 0.8 Supra at 20 °C.**

**Table 4. Pore distribution of Silicarbon 0.8 Supra**

| <6 nm | 6-10 nm | 10-16 nm | 16-20 nm | 20-80 nm | >80 nm |
|---|---|---|---|---|---|
| 52.4% | 13% | 9.7% | 8.6% | 16.8% | 4.5% |

hardly adsorb water vapor at lower pressures due to the hydrophobic nature of carbon. At a pressure ratio above 0.6, a significant increase in the isotherm is caused by capillary condensation in large pores. Large macropores cannot become completely filled; however, the isothermal curve flattens off at a pressure ratio above 0.8, in the vicinity of the maximal impregnation of 45% v/v. The pore distribution of Silicarbon is shown in Table 4.

It is worth mentioning that the perpendicular cross section of a water molecule is $10.6\times10^{-20}$ m$^2$, so in a limiting case a water molecule can fit in pores with a diameter of 0.367 nm, though in reality this limit is approximately 1 nm. However, in practice the water molecule cannot get into the submicron pores of the activated carbon ($d_p$<1 nm). As can be seen in Table 4, the Silicarbon brand activated carbon contains only a relatively small proportion of macropores ($d_p$>80 nm). Pore distribution and the associated pore volume are highly affected by the wet impregnation.

## RESULTS AND DISCUSSION

### 1. Phase Holdups and Bed Expansion

It is known that the expansion of a fluidized bed can be defined by the ratio of actual bed height to fixed bed height, density of the bed and the average voidage factor, which is defined as volume of void space divided by the total volume of the bed. This final parameter cannot be measured directly; it must be calculated from the data obtained by various measurement methods [19].

By definition:

$$\varepsilon_f+\varepsilon_s=1 \tag{1}$$

$$\varepsilon_s=\frac{M}{H_0 S\rho_s}=\frac{\rho_B}{\rho_a} \tag{2}$$

In case of activated carbon, $\rho_s$ is only the apparent and not the true density, i.e., $\rho_s=\rho_a$. If the apparent density is higher than that of the fluidization medium, then a classical, upward-flowing medium can be used. In this case, the pressure drop of the fluidized bed is:

$$\frac{\Delta P}{H_0}=(1-\varepsilon_f)(\rho_a-\rho_f)g \tag{3}$$

But if $\rho_a<\rho_f$, the bed becomes an inverse fluidized, and in this case:

$$\frac{\Delta P}{H_0}=(1-\varepsilon_f)(\rho_f-\rho_a)g \tag{4}$$

The pressure drop of Eqs. (3) and (4) would be constant at $u\geq u_{mf}$. To determine the bed size, temperature dependency of the parameters such as the density and viscosity of the liquid must also be taken into account.

The apparent density of activated carbon can be determined when the true density and the pore volume are known. Using the data from Table 1 for the case of Silicarbon 0.8 Supra, calculating from the true density, the volume of the structural framework of 1 g carbon is 0.465 cm$^3$ and the volume of the internal pores is 0.62 cm$^3$. The sum of these two volumes is 1.085 cm$^3$, and hence the apparent density is $\rho_a$=0.9216 g/cm$^3$ so the IFB pressure drop of the activated carbon can now be determined by using Eq. (4).

During the wet impregnation, water penetrates into the pores of the carbon, so the particles become heavier. The apparent density of activated carbon changes due to the impregnation of the vesicles, as shown in Table 5. It is to be noted that no publication on this special change has been found in the liquid fluidization literature. Table 5 shows the impregnation of macropores and intermediate pores larger than 20 nm that changes the balance of forces acting on the particles in the two-phase medium. According to the laws of dynamics, a body immersed in a liquid will rise or fall, experiencing acceleration until its velocity is stabilized as a result of increasing drag in the direction opposite to the movement. The limiting velocity or particle terminal velocity is determined by the well-known expression as $u_t=[(4d(\rho_f-\rho_s)g)/(3C_D\rho_f)]^{1/2}$ where $C_D$ is the drag coefficient dependent on the Re number. As the impregnation of carbon particles increases, so the density difference between the water and carbon decreases. When the apparent density of the activated carbon reaches the density of water, the particles will begin to float and the flowing liquid will push the layer to the top or bottom grid, depending on the direction of the flow. If impregnation continues, the particles become heavier than water and the layer can be fluidized in the classical way, by water flowing upwards.

Since the pressure drop in the fluidized bed is invariant with the flow rate above $u_{mf}$, the density decrease $(\rho_f-\rho_a)$ is compensated by the decrease in $\varepsilon_f$. A lower voidage factor is naturally associated

**Table 5. Change of apparent density by impregnation**

| Pore diameter nm | Pore volume % | $\rho_a$ g/cm$^3$ |
|---|---|---|
| >80 | 0 | 0.9216 |
| >20 | 4.5 | 0.947 |
| >20 | 4.5+16.8 | 1.043 |
| >6 | 47.6 | 1.123 |
| <6 | 100 | 1.51 |

with a lower bed height. It was observed that the expanded fluidized bed height of 1.36 m dropped to 1.26 m with the microwave treatment. When the activated carbon becomes heavier than water, the difference of $(\rho_a-\rho_f)$ also increases with impregnation, so $\varepsilon_f$ and the expanded bed height will also increase in a manner typical of classical fluidization. The distinctive changes outlined above are the reason for alternating the circulation of water through the column during the impregnation process.

It should be noted that the inversion in density difference described above may also occur at a lesser degree of impregnation, if upward bubbling air released from vesicles in the carbon is considered as a third phase. In our case, the volume of this was 3,100 $cm^3$ and the forward slip is 0.6-1.6 m/s. Based on the principle of the air-lift or mammoth pump, the density of the water/air mixture decreases in proportion to the quantity of air bubbles, and the difference as compared to the apparent density of carbon also decreases.

Knowing the apparent and bulk densities of the bed, the fixed bed voidage factor is $\varepsilon_o=1-\rho_B/\rho_a=0.513$. The fixed bed height of the activated carbon was 0.8375 m in the column (0.130 m-ID). The effective voidage of the fluidized bed is therefore $\varepsilon_e=(H_{fl}-H_0)/H_0=0.6238$ and the bed voidage factor is

$$(1-\varepsilon_{fl})=\frac{1-\varepsilon_0}{\varepsilon_e+1} \tag{5}$$

where $\varepsilon_{fl}=0.701$

Several equations have been published for bed expansion in a liquid/solid IFB [8,9,12]. Due to the large particle size (d>6 mm), the validity range of the equations for Ar in the first two publications was broader than that in the present study, so these could not be used in our study. On the other hand, the authors of the third publication used the widely accepted Richardson-Zaki [20] equation as:

$$u/u_t=\varepsilon^n. \tag{6}$$

Eq. (6), as Eq. (11) was used also by Lee [11]. In his paper the values of the spherical non-vesicular particles varied from 3.2 to 6.0 mm. Analyzing the published 12 types of water-fluidized systems, Garside and Al-Dibouni [10] reported that the Richardson-Zaki [20] equation corresponds well with their measurement data in case of the bed voidage, $\varepsilon<0.9$. As the bed voidage is lower than 0.9 in the present study, Eq. (6) was used to characterize the IFB layer. In the present study, the Reynolds numbers are in the range of $1<Re_t<200$, and n is given by $n=(4.45+18d/D)Re_t^{-0.1}$.

Due to the low value of d/D=0.0028 in our case, the wall effect can be neglected and the calculations are made based on the assumption that $u_i=u_t$.

$$Re_t=0.152Ar^{0.715} \tag{7}$$

where $Re_t=u_td/\nu$ in the range of $4<Re_t<400$.

For the case of Silicarbon 0.8 Supra, $Re_t=26.0$, $u_t=0.0227$ m/s and n=3.215.

In our fluidization measurements: $u=u_{fl}=0.00837$ m/s at $Re_{fl}=9.5$

Substituting the above results in Eq. (6), the voidage factor of the IFB is $\varepsilon=\varepsilon_{fl}=0.729$, which is acceptably close to 70.1% from the visual observation.

For the Silicarbon 0.8 Supra, $\varepsilon=\varepsilon_{mf}=0.513$ and n=3.215, $u_{mf}=0.00265$ m/s and the associated $Re_{mf}$ is 3.03. A depiction of the $\varepsilon$ and Re numbers listed above in the log Re vs. log $\varepsilon$ system is shown in Fig. 3. It can be seen that the measured points lie along the expected straight line with a good approximation.

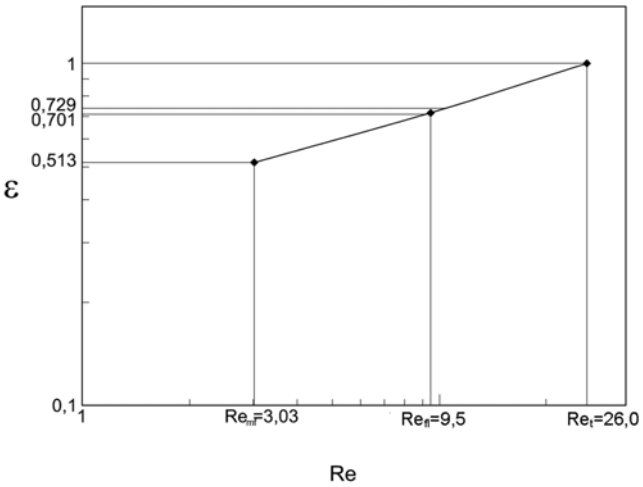


**Fig. 3. Reynolds number vs. voidage in a bed of Silicarbon fluidized by water.**

**2. Critical fluidization velocities ($u_{mf}$ and $u_t$)**

The MFV, minimum fluidization velocity ($u_{mf}$) can be determined from Eq. (3) or (4). The Ergun equation is very widely used to determine the pressure drop of fixed bed gas/solid systems:

$$\frac{\Delta P}{H_0}=C_1\frac{\mu(1-\varepsilon_0)}{d^2\varepsilon_0^3}u+C_2\frac{\rho_f(1-\varepsilon_0)}{d\varepsilon_0^3}u^2 \tag{8}$$

Ergun [21] established the constants $C_1$ and $C_2$ based partially on his own data and partially on those found in the literature. The constant $C_1$ is 150 but $C_2$ varied widely between 1.2 and 3.9, so $C_2$= 1.75, as is given by Ergun [22] and also by Lee [11], is an incorrect average value.

To clarify this matter, experiments were carried out using spheres of various sizes and made of five different materials in a fixed bed [18]. At higher velocities, i.e., when the second term on the right hand side of Eq. (8) is dominant, measurement points were found to be 10-12% lower than the calculated values. By linearizing Eq. (8)

$$f=C_1+6C_2Re_3 \tag{9}$$

where the friction coefficient is $f=[(\Delta Pd^2\varepsilon_0^3)/H_0\mu(1-\varepsilon_0)^2]/(1/u)$ and $Re_3=d_h\cdot v/\nu=d\cdot u/[6\nu(1-\varepsilon_o)]$. In the previous expression, $d_h$ is Kozeny's hydraulic diameter, and v is the actual velocity between the particles.

When Eq. (9) was fitted to the measured points by the least squares method, the following values of the two constants were obtained:

$C_1=150$ and $C_2=1.45$

Consequently:

$$f=150+1.45Re_2 \tag{10}$$

where $Re_2=6\ Re_3=u\cdot d/[\nu(1-\varepsilon_o)]$. It should be noted that $Re_2$ is used quite frequently to characterize agglomerates of vesicular particles [6,9,13].

The pressure drop data for air-fluidized activated carbon of Hun-

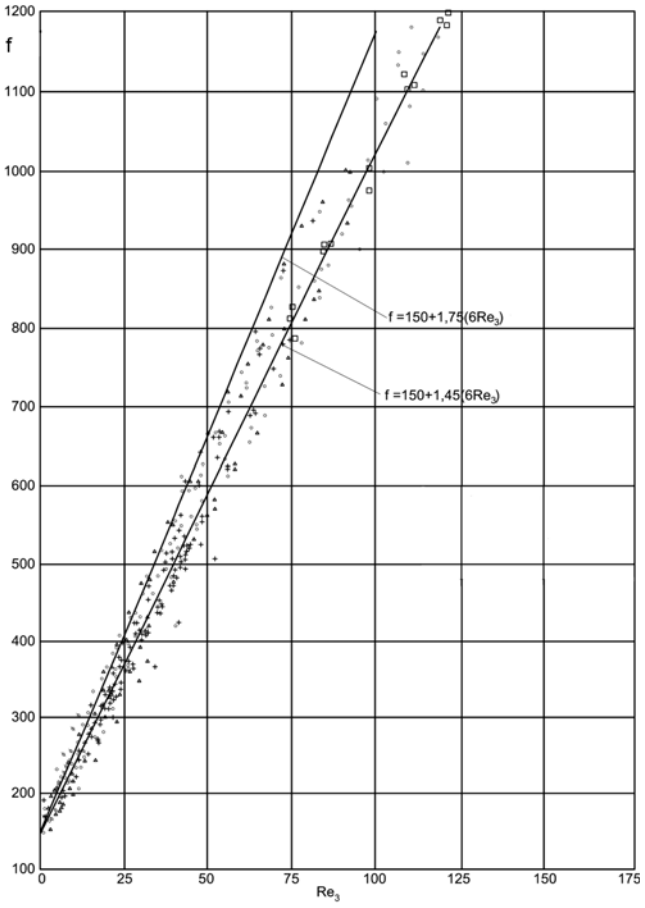


**Fig. 4. Friction factor vs. $Re_3$ number in fixed bed of spherical particles.**

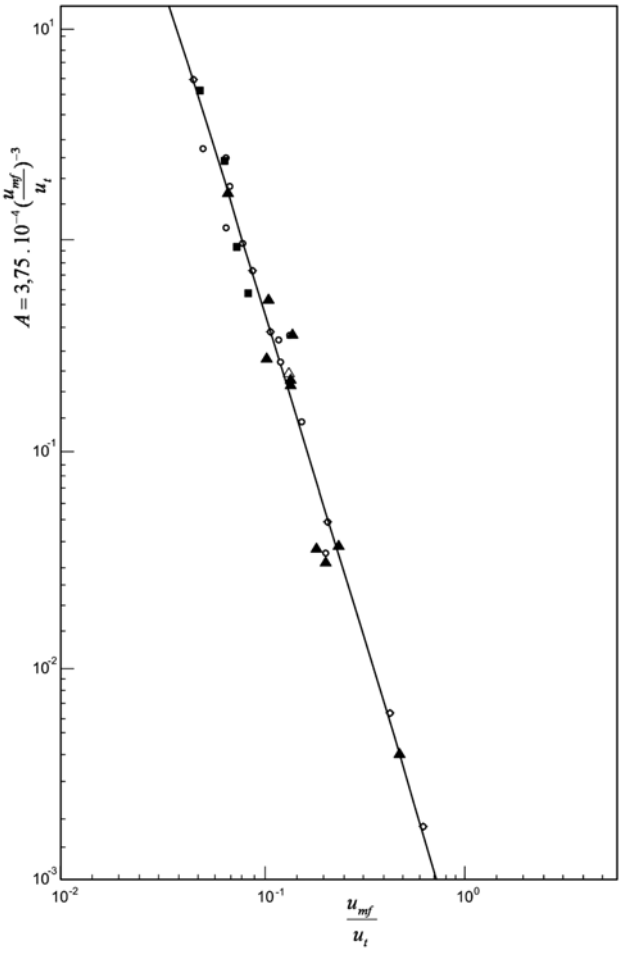


**Fig. 5. Values of A vs. velocity simplex of $u_{mf}/u_t$.**

garian "Nuxit BO" was plotted according to Eq. (10). The measured data only fit to the original Ergun equation at lower flow rates, but they fit the straight line of the adjusted Eq. (10) well over the whole measurement range. For the activated carbon measurements $d=\psi\bar{d}$ where $\psi$ is the shape factor which is given in Table 3.

Examining the relationship between $Re_{mf}$ and Ar numbers in the inverse fluidization, Karamanev and Nikolov [23] found that their measurement data were lower than the values calculated by the Ergun equation at $Re_{mf}$ value greater than 30-40 by an amount similar to those in Fig. 4.

Using Re and Ar numbers, Eq. (10) with $\varepsilon$=0.4 can be changed as:

$$Re_{mf}^2+62.1Re_{mf}-0.044Ar=0 \quad (11a)$$

The minimum fluidization velocity $u_{mf}$ can be obtained by solving the quadratic Eq. (10) or (11a).

Utilizing the original Ergun equation with a value of $\varepsilon$=0.4, Richardson [24] has given the following expression:

$$Re_{mf}^2+51.4Re_{mf}-0.036Ar=0 \quad (11b)$$

It can be seen that in the last two equations, the values of the second and the third terms only differ because of the differing $C_2$ values.

To ensure the use of correct dimensions, it is often desirable to measure the hydrodynamic parameters of a given system experimentally. Therefore, Blickle and Németh [25] proposed for designing the basic data of $u_{mf}$ and $u_t$ determined experimentally. Analyzing experiments with 12 different materials, including Nuxit activated carbon and 15 gas/solid systems from six sources in the literature, they obtained the following equation for the pressure drop in a fixed bed:

$$\Delta P=\frac{Mg}{S}\left[\left(\frac{1}{u_{mf}}-0.000375\frac{u_t^3}{u_{mf}^2}\right)u+0.000375\frac{u_t^3}{u_{mf}^3}u^2\right] \quad (12)$$

By introducing $A=3.75\times10^{-4}(u_{mf}/u_t)^{-3}$, it can be seen that the experimental data are located along the straight line (Fig. 5). Because of this straight line, there is good reason to assume that the data from other pairs of materials will also fit the straight line. For the activated carbon in Table 3, the $u_{mf}$ and $u_t$ data as well as the A values are shown in Table 6.

At the end of the paper, the relationship of the Ar-Re numbers should be summarized.

**Table 6. The $u_{mf}$ and $u_t$ values of Nuxit BO**

| | | | | |
|---|---|---|---|---|
| $\bar{d}$, mm | 0.408 | 0.715 | 0.90 | 1.8 |
| $u_{mf}$, m/s | 0.062 | 0.15 | 0.39 | 0.76 |
| $u_t$, m/s | 1.13 | 2.156 | 2.79 | 4.06 |
| A | 2.27 | 1.11 | 0.137 | 0.057 |

First, the data obtained from a large number of experiments with solid/gas and solid/water systems were depicted by Wilhelm and Kwauk [26] in the co-ordinate system $K_{\Delta\rho}$=0.5Ar vs Re. The obtained data of minimum fluidization velocity of the same particles fluidized by both air and water fell on the same curve. In their experiments, density of the particles was always greater than that of the fluid.

The curves in Fig. 6 taken from Gelperin [27] was applied to an air-fluidized bed, where $\rho_s > \rho_f$, so the density difference in Ar number is $(\rho_s - \rho_f)$, and the voidage ($\varepsilon$) is 0.4.

Renganathan and Krishnaiah [28] proposed the Re and Ar relationship in the inverse water-fluidized bed as shown in Fig. 7 that corresponds to Eq. (13) with $\varepsilon$=0.4.

$$Re_{mf}=[33.7^2+0.0408Ar]^{0.5}-33.7 \quad (13)$$

In the figure, the data of 14 publications were compared using the modified Ar number in which the density difference $(\rho_f - \rho_s)$ was used in contrast to the original Ar number. According to the authors, "the equation used for MFV in classical fluidized beds is expected to be valid as well as in the inverse fluidized beds." For two-phase (L-S) systems, Lee [11] demonstrated experimentally that MFV should be the same for both upward and downward fluidization systems.

If the axes of Figs. 6 and 7 are adjusted to the same scale, and the two groups of curves charted together, we can draw Fig. 8. As can be seen, the curves of classical air-fluidized bed systems and those of IFB systems have a common form as expected by Renganathan and Krishnaiak [28]; the $Re_{mf}$ points associated with the original and the modified Ar numbers lie along the same curve.

Todes and Tzitovich [29] show the $Re_{mf}$ relationship with the bed voidage of 0.48 and 0.4 as shown in Fig. 9. It can be seen that at an identical Ar number, a higher $Re_{mf}$ is associated with a higher voidage factor. The same was obtained in the present study in the case of $\varepsilon_o$=0.513, $Re_{mf}$=2.47 with a value of Ar=1139.

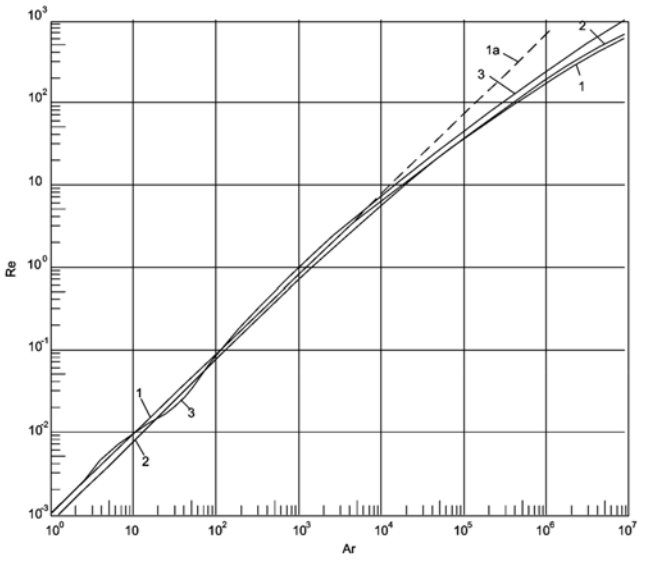


**Fig. 6. Ar number vs. Re number at minimum fluidizing condition. (1) and (1a) Leva [30], (2) Gelperin et al. [27], (3) Beranek et al. [31].**

## CONCLUSION

Liquid was circulating through the bed with activated carbon that

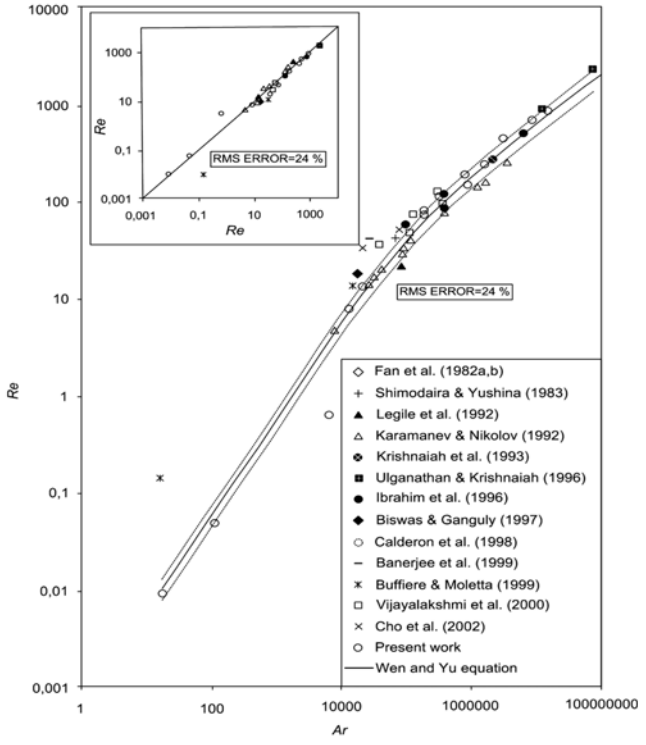


**Fig. 7. Modified Ar number vs. liquid Re number at minimum fluidizing condition.**

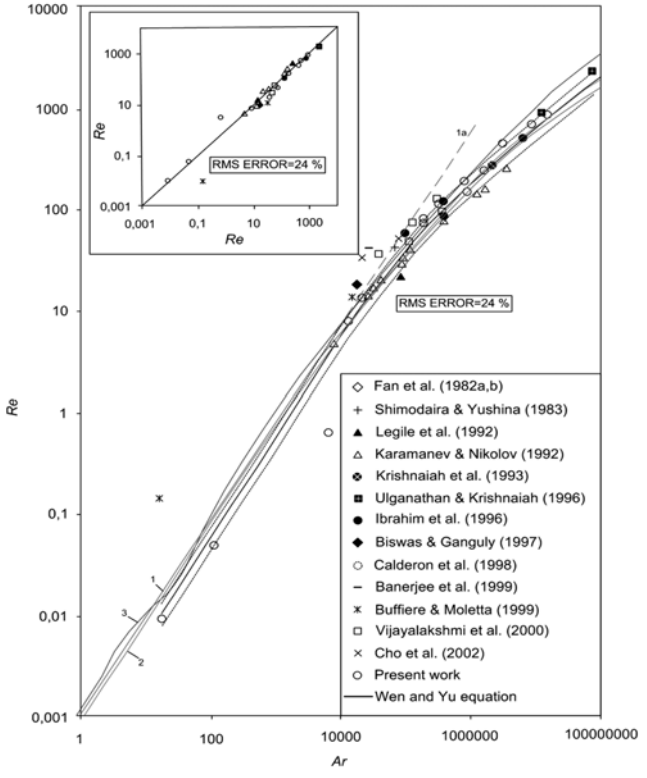


**Fig. 8. Combined diagram of Figs. 6 and 7.**

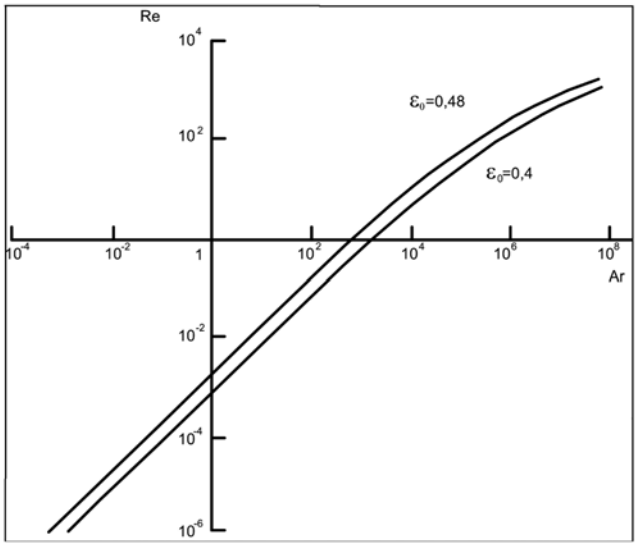


**Fig. 9. Ar number vs. Re number at the minimum fluidizing condition for various void fractions.**

was fed either at the top or at the bottom of the column to form an inverse or a classical fluidized bed.

The hydrodynamic characteristics (phase holdup and bed expansion) of the fixed, inverse or a classical fluidized beds of four different activated carbons having small particle size and low apparent densities were determined. The fluidizing system switches over from the inverse fluidized bed into the classical fluidized state when the macropore and the meso-pores, larger than 20 nm of the activated carbon particles, become saturated with water.

Based on the present experimental data, the Ergun-equation was corrected. For the calculation of the pressure drop of gas flowing through a fixed bed, a new relationship is proposed by using the experimentally data of $u_{mf}$ and $u_t$. The inverse liquid/solid fluidized beds can be characterized by $Re_{mf}$ associated either with the original Ar number for gas/solid fluidized systems or the modified Ar number, if $\rho_a<\rho_f$.

## NOMENCLATURE

A : $A=3.75\times10^{-4}\,(u_{mf}/u_t)^{-3}$ [-]
Ar=$(gd^3\Delta\rho\cdot\rho_f)/\mu^2$ : Archimedes number [-]
D : diameter of the column [m]
$H_o$ : initial bed height [m]
$H_{fl}$ : fluidized bed height [m]
M : weight of solid particles [kg]
$Re_{mf}=u_{mf}d/\nu$ : Reynolds number at minimum fluidization [-]
$Re_t=u_td/\nu$ : Reynolds number at terminal condition [-]
$Re_2$ : Reynolds number defined by $du/(\nu(1-\varepsilon_0))$ [-]
$Re_3$ : Reynolds number defined by $du/(6\nu(1-\varepsilon_0))$ [-]
S : cross sectional area of the column [$cm^2$]
d : diameter of particle spheres [mm]
$\overline{d}$ : average diameter of activated carbon [mm]
$d_p$ : pore diameter of activated carbon [nm]
f : friction factor [-]
g : gravitational acceleration [$m\cdot s^{-2}$]
u : superficial velocity [$m\cdot s^{-1}$]
$u_{mf}$ : minimum fluidizing velocity [$m\cdot s^{-1}$]
$u_t$ : terminal velocity of a particle [$m\cdot s^{-1}$]
v : actual velocity of the fluid [$m\cdot s^{-1}$]

### Greek Letters

$\varepsilon$ : average void fraction of the bed [-]
$\varepsilon_e$ : effective bed voidage [-]
$\varepsilon_o$ : bed-voidage at the minimum fluidizing condition [-]
$\varepsilon_f$ : liquid holdup [-]
$\varepsilon_{fl}$ : liquid holdup of fluidized bed [-]
$\varepsilon_{mf}$ : liquid hold up at minimum fluidizing velocity [-]
$\varepsilon_s$ : solid holdup [-]
$\rho_a$ : apparent density of activated carbon [$g\cdot cm^{-3}$]
$\rho_B$ : bulk density of the bed [$g\cdot cm^{-3}$]
$\rho_f$ : density of fluid [$g\cdot cm^{-3}$]
$\rho_s$ : solid density [$g\cdot cm^{-3}$]
$\rho_T$ : solid true density [$g\cdot cm^{-3}$]
$\mu$ : fluid viscosity [$kg\cdot m^{-1}\cdot s^{-1}$]
$\nu$ : kinematic viscosity of fluid [$m\cdot s^{-2}$]
$\psi$ : particle shape factor [-]

## REFERENCES

1. D. Kunii and O. Levenspiel, *Fluidization engineering*, Wiley, N.Y. (1969).
2. A. Anderson, S. Sundaresan and R. Jackson, *J. Fluid. Mech*., **303**, 327 (1955).
3. Y. J. Cho, H. Y. Park, S. W. Kim, Y. Kang and S. D. Kim, *Ind. Eng. Chem. Res*., **41**, 2058 (2002).
4. H. D. Han, W. Lee, Y. K. Kim, J. L. Kwon, H. S. Choi, Y. Kang and S. D. Kim, *Korean J. Chem. Eng.*, **20**, 163 (2003).
5. L. S. Fan, *Gas-liquid-solid fluidization engineering*, Butterworth, Boston, Stoneham, MA (1989).
6. A. C. V. Lakshmi, M. Balamurugan, M. Sivakumar, T. N. Samuel and M. Velan, *Bioprocess Eng.*, **22**, 461 (2000).
7. L. S. Fan, K. Muroyama and S. H. Chern, *Chem. Eng. J*., **24**, 143 (1982).
8. N. Ulaganathan and K. Krishnaiah, *Bioprocess Eng*., **15**, 159 (1995).
9. R. J. F. Bendict, G. Kumaresan and M. Velan, *Bioprocess Eng.*, **19**, 137 (1998).
10. J. Garside. and M. Al-Dibouni, *Ind. Eng. Chem. Process Des. Dev*., **16**, 206 (1997).
11. D. H. Lee, *Korean J. Chem. Eng.*, **18**, 347 (2001).
12. T. Renganathan and K. Krishnaiah, *Chem. Eng. Sci*., **60**, 2545 (2005).
13. Y. Kato, K. Ushida, T. Kago and S. Morooka, *Powder Technol*., **28**, 173 (1981).
14. M. P. Comte, D. Bastoul, G. Hebrard, M. Roustan and V. Lazarova, *Chem. Eng. Sci.*, **52**, 3971 (1997).
15. N. Epstein, D. H. Lee, A. Macchi and J. R. Grace, *Chem. Eng. Sci*., **56**, 6031 (2001).
16. J. Németh and T. Virág, *Acta Chimica Hungarica*, **115**, 273 (1984).
17. E. W. Lewis and E. W. Bowerman, *Chem. Eng. Progr.*, **48**, 63 (1952).
18. J. Németh and L. Imre, *Design of drying by adsorption*, (in Hungarian), in "Handbook of Drying," Chapter 14, Müszaki KK., Budapest (1974).
19. Z. Ormós, *Hung. J. Ind. Chem*., **1**, 31 (1973).
20. J. F. Richardson and W. N. Zaki, *Trans. Inst. Chem. Engrs*, **32**, 35

(1954).
21. S. Ergun and A. A. Orning, *Ind. Eng. Chem*., **41**, 1179 (1949).
22. S. Ergun, *Chem. Eng. Progr.*, **48**, 89 (1952).
23. D. G. Karamanev and N. Nikolov, *AIChE J*., **38**, 1916 (1992).
24. J. F. Richardson, *Transient fluidization and particulate systems*, in "Fluidization," J. F. Davidson and D. Harrison, Eds., Academic Press N.Y., p. 39 (1971).
25. T. Blickle and J. Németh, *Acta Chimica Hungarica*, **67**, 113 (1971).
26. R. H. Wilhelm and M. Kwauk, *Chem. Eng. Progr.*, **44**, 201 (1948).
27. N. I. Gelperin, V. G. Ainstein and V. B. Kvasha, *Basics of fluidization techniques*, (in Russian), Chemistry, Moskow, p. 84 (1967). "Chemists' Handbook," Ed.: Nikolsky, B.P. (in Russian), Chemistry, Moskow (1966).
28. T. Renganathan and K. Krishnaiah, *Can. J. Chem. Eng*., **81**, 853 (2003).
29. O. M. Todes and O. B. Tzitovich, *Vessels containing fluidized layers* (in Russian), Chemistry, Leningrad (1981).
30. M. Leva, *Fluidization*, McGraw-Hill Co., N.Y., p. 64 (1959).
31. J. Beranek, D. Sokol and G. Winterstein, *Wirbelschichttechnik* (in German), Leipzig (1964).